A Comprehensive Explanation of Distortion Sideband Asymmetries

Nuno Borges de Carvalho, *Member, IEEE,* and José Carlos Pedro, *Senior Member, IEEE*

***Abstract*—This paper presents a comprehensive study of intermodulation-distortion response asymmetries often observed in microwave nonlinear systems subject to a two-tone or multitone test. The reasons for the different amplitudes of the two adjacent tones are first investigated under small- and large-signal regimes, using a general circuit with frequency-dependent embedding impedances and resistive and reactive nonlinearities. It is shown that this intriguing phenomenon can be mainly attributed to the terminating impedances at the baseband or difference frequencies. Multitone behavior is also addressed and its main differences from the two-tone case explained. Those theoretical conclusions are then extrapolated for real circuits and validated by measured results obtained from microwave power amplifiers of two different technologies, i.e., a GaAs MESFET and an Si bipolar junction transistor.**

***Index Terms*—Amplifier distortion, describing functions, multitone signals, nonlinear circuits, Volterra series.**

I. Introduction

ASYMMETRIES in the amplitudes of lower and upper intermodulation distortion (IMD) tones are often observed in real microwave devices subject to two-tone or multitone tests [1]–[6]. That is, two-tone IMD power associated to the $2\omega_2 - \omega_1$ response component is distinctly different from the one at $2\omega_1 - \omega_2$. In a multitone signal, this effect is observed when the low adjacent channel power ratio (ACPR) is distinct from the upper ACPR.

Beyond the scientific curiosity such an intriguing phenomenon creates, it may also be the direct cause of misjudgments when measuring intermodulation ratio (IMR) third-order intercept point (IP_3), and other commonly used distortion figures-of-merit. Since these specifications were defined for the ideal case of exactly equal adjacent tones, the microwave engineer may get confused when facing asymmetric IMD responses. Which IMR or IP_3 values should he report if his microwave power amplifier (PA) presents lower and upper IMD figures as different as 6 dB?

From a modeling point-of-view, these asymmetries can degrade, or even induce in error, the extraction of different model parameters.

Finally, these asymmetries can also perturb the correct behavior of predistortion amplifiers when designed using a one-tone AM–AM or AM–PM characteristic since the IMD upper sideband will be more or less compensated than the lower one [1]. In general, the correct design of any amplifier linearizer requires a correct understanding of this behavior and the knowledge of how to generate and control it, otherwise circuits' specifications may be met in one of the IMD sidebands, but failed in the other one.

Another interesting matter regards the causes for IMD asymmetry. Which are the mechanisms that create it and how can it be controlled or avoided are two questions of undeniable importance if we want to have a clearer view of the impact of nonlinearities in microwave devices or simply get better results when measuring those IMD figures-of-merit.

Previously published works have already dealt with this problem [1]–[6], attributing asymmetric third-order IMD amplitude to various types of memory effects in PAs.

Bosch and Gatti [1] related the IMD large-signal behavior to the biasing networks and have experimentally demonstrated that this effect can dramatically alter the correct operation of a predistortion amplifier.

Sevic *et al.* [2] have experimentally observed that the envelope termination can unbalance upper and lower ACPRs in a multitone large-signal amplifier. For that, an experimental envelope load–pull has been undertaken, which allowed the relation of ACPR asymmetry variations to this low-frequency-output load impedance.

Aparin and Persico [3] have also seen this effect in a bipolar junction transistor (BJT) amplifier and, by using a relatively simple small-signal model, have related its causes to the out-of-band terminations.

Secchi [4] has observed this phenomenon in a high-efficiency linear PA and directed the explanation of this behavior to either the limitation of the modulation bandwidth or, instead, to an inevitable unbalance of the two input signal drive levels.

Recently, Borges de Carvalho and Pedro [5] have mathematically proven that the small-signal two-tone IMD asymmetry can be attributed to the biasing matching networks. This constituted a theoretical confirmation of many of the hypotheses previously anticipated [1]–[4]. However, it also supports experimental observations [6]. In that respect, it is worth telling that the conclusions drawn in [5] for the relation of IMD asymmetries and load termination at the baseband can easily be extrapolated to incorporate the baseband memory effects due to low-frequency dispersion or self heating [7].

The main objective of this paper is to present a comprehensive study of this phenomenon and, thus, to reveal its origins under small- and large-signal two-tone and multitone excitations.

For that, in Section II, a single-node nonlinear circuit composed of a frequency-dependent terminating impedance

Manuscript received June 18, 2001. This work was supported by the Portuguese Science Bureau, F.C.T. under Project PRAXIS/C/EEI/14160/1998-LINMIX.

The authors are with the Instituto de Telecomunicações, Universidade de Aveiro, 3810-193 Aveiro, Portugal (e-mail: nborges@ieee.org; jcpedro@ieee.org).

Publisher Item Identifier 10.1109/TMTT.2002.802321.

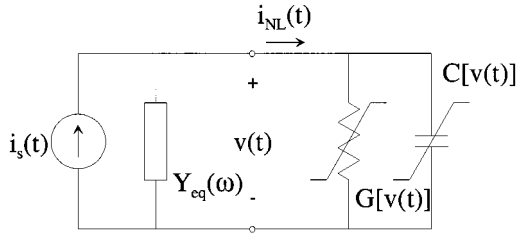

Fig. 1. Simple general circuit for IMD asymmetry analysis.

and resistive and reactive nonlinear components is analyzed both in small- and large-signal regimes. Necessary conditions for small-signal IMD asymmetry are derived. Special emphasis is put on studying the impact of baseband (or difference frequency) terminating impedances and active device bias points. Section III deals with multitone excitations and its specific related problems. Section IV validates these theoretical conclusions using laboratory measurement results obtained from microwave PAs operated in a broad range of quiescent points, tone separation, and drive level for two different technologies, i.e., a GaAs MESFET and an Si BJT. Finally, Section V summarizes the most important conclusions of this study.

II. Simple General Circuit Analysis

A. Two-Tone Small-Signal Circuit Analysis

In [5], the authors have already discussed the mechanisms causing IMD asymmetry under two-tone (at ω_1 and $\omega_2 : \omega_2 > \omega_1$) small-signal operation for a simple general circuit. Therefore, here, we will only summarize those conclusions.

For the general theoretical analysis carried on, the circuit of Fig. 1 was considered, as it represents the best compromise between analysis simplicity—it is composed of a single node—and completeness—its nonlinear elements include resistive and reactive nonlinearities. Also, its linear embedding admittance $Y_{\rm eq}(\omega)$ shows frequency-dependent resistive and reactive parts.

Since small-signal nonlinear dynamic behavior was sought, the circuit analysis technique used was the nonlinear currents method of Volterra series [8]. From that, the following major conclusions were drawn.

1) The presence of a significant reactive part on the baseband termination (e.g., $Y_{\rm eq}(\omega_2 - \omega_1)$ in a two-tone test) is a necessary condition for IMD asymmetry.
2) Third-order mixing products, directly arising from third-degree coefficients of the nonlinearities' Taylor series approximations, cannot be so large as to mask third-order IMD generated by remixing the fundamentals with second-order distortion in second-degree coefficients. IMD asymmetry is thus bias sensitive and manifests itself in a great extent near small-signal IMD sweet spots.
3) Real parts of terminations presented to the second harmonic and baseband cannot dominate over reactive parts.
4) Imaginary parts of baseband and second harmonic terminations should have comparable magnitudes. The interaction between those two determine IMD asymmetry in circuits commonly found in practice. A very intuitive graphical illustration of this interaction, using vector magnitude additions was already proposed by Sevic *et al.* [2].
5) If second harmonic termination is resistive, IMD asymmetry can still be observed in presence of an important reactive nonlinearity.

B. Two-Tone Large-Signal Circuit Analysis

Although the above analysis provides a good insight to the deep origins of IMD asymmetries in a small-signal regime, it can be of little use to practical PAs. Indeed, due to efficiency considerations, not only usual microwave PAs are operated in large-signal regimes, as they are biased with reasonably low quiescent currents. There, direct third-degree mixing is often hardly negligible compared to the IMD generated by the second-degree coefficients, which violates the second condition. Nevertheless, IMD asymmetries can still be found in large-signal IMD sweet spots, as will be shown below.

The circuit used for large-signal analysis is still the one shown in Fig. 1, except that now only the resistive nonlinearity is considered. Due to the difficulty of Volterra series in describing large-signal behavior, $G[v(t)]$ can no longer be approximated by a Taylor series and the full algebraic expression must be used for the nonlinear current

$$I_{\rm NL}(t) = f_{\rm NL}\big[I_s(t)\big]. \tag{1}$$

This hypothetical nonlinearity must be one that includes cutoff and saturation to closely represent the expected behavior of usual PAs.

To study the IMD under a large-signal regime, the behavioral model presented in [9] was used as follows:

$$I_{\rm NL}\,(2\omega_2 - \omega_1) = SS\,(A, 2\omega_2 - \omega_1) + LS\,(A, 2\omega_2 - \omega_1) \tag{2a}$$

$$I_{\rm NL}\,(2\omega_1 - \omega_2) = SS\,(A, 2\omega_1 - \omega_2) + LS\,(A, 2\omega_1 - \omega_2) \tag{2b}$$

where SS and LS denote the small- and large-signal response behaviors, as explained in [9].

This behavioral model separates the complete analysis in two descriptions: the small signal, modeled by a Volterra series and the large signal given by the describing function [10].

Approximate information concerning large-signal IMD behavior can be gathered from the relation between output fundamental signal $S(A)$ and distortion power $I(A)$ as a function of driving amplitude A in a memoryless nonlinear system [10]

$$I(A) = S(A) - \frac{4}{A^3}\int_0^A x^2 S(x)dx. \tag{3}$$

Limited available supply power and energy conservation in our nonlinear system determine an output power saturation constraint, which maybe expressed as $\lim_{A\to\infty} S(A) = S_s$ (constant).

The substitution of this condition into (3) gives the result

$$I(A) = -\frac{1}{3}S_s \tag{4}$$

which means that the large-signal asymptotic behavior of IMD in any memoryless nonlinear system is such that it also saturates to a constant value 9.54 dB below the fundamental signals and opposite in phase to them.

With these ideas in mind and with the aid of the behavioral model of (2a) and (2b), we can consider the following description for the upper and lower large-signal IMD:

$$\mathrm{IMD}_U = V_R(2\omega_2 - \omega_1) + jV_I(2\omega_2 - \omega_1) - V_A(2\omega_2 - \omega_1) \tag{5}$$

$$\mathrm{IMD}_L = V_R(2\omega_1 - \omega_2) + jV_I(2\omega_1 - \omega_2) - V_A(2\omega_1 - \omega_2) \tag{6}$$

where IMD_U and IMD_L are the upper and lower intermodulation voltages, $V_R(\omega_{\mathrm{IMD}})$ is the real part of those voltages, $V_I(\omega_{\mathrm{IMD}})$ is the corresponding imaginary parts, and $V_A(\omega_{\mathrm{IMD}})$ is the referred asymptotic large-signal contribution.

Since $V_R(\omega_{\mathrm{IMD}})$ and $V_A(\omega_{\mathrm{IMD}})$ are equal for the upper and lower bands, it may be concluded that, according to what was already proven for small- and large-signal IMD asymmetries can only be caused by differences in the imaginary parts of the IMD.

Another interesting statement of the previous section was that small-signal IMD asymmetry would only be visible if the real part of IMD components did not override their imaginary parts. Since in the asymptotic very large-signal operation, IMD tends to be real and negative, i.e., in opposite phase to the output linear components, large-signal IMD asymmetries may only take place in zones where the dominant real part is cancelled out. Such zones exist, in fact, for certain bias points and signal excitation levels and where studied and named large-signal IMD sweet spots, as in [9]. Therefore, an important conclusion to be drawn is that large-signal IMD asymmetries will only be evident in large-signal IMD sweet spots and provided that baseband and second harmonic terminations are reactive. Also, similar to what was already observed in the small-signal regime, the amount and direction of large-signal IMD asymmetries will be determined by the values of the imaginary parts of upper and lower IMD components.

To deeply explain and validate these hypothesis, let us discuss a particular case of our test circuit, for which the characteristic function—node voltage $v(t)$, versus source current $i_s(t)$—is depicted in Fig. 2(a).

In order to develop the desired circuit's small-signal Volterra-series model, that nonlinear characteristic function was first expanded in a Taylor series, whose coefficients' values are represented in Fig. 2(b).

For exploring all distinct IMD qualitative behaviors that may appear in such a nonlinear circuit [9], its nonlinearity was biased at three different quiescent points: $R_{c3} = 0$, an IMD small-signal sweet spot ($I_S = 60$ mA), positive R_{c3} for the generation of a large-signal IMD sweet spot ($I_S = 20$ mA), and at a negative R_{c3}, where third-order small-signal IMD components are in-phase with large-signal IMD and so no kind of IMD sweet spot is possible ($I_S = 70$ mA).

The load impedance was considered to be highly reactive for the baseband ($\omega_2 - \omega_1$) and second harmonic ($2\omega_1$ or $2\omega_2$) and

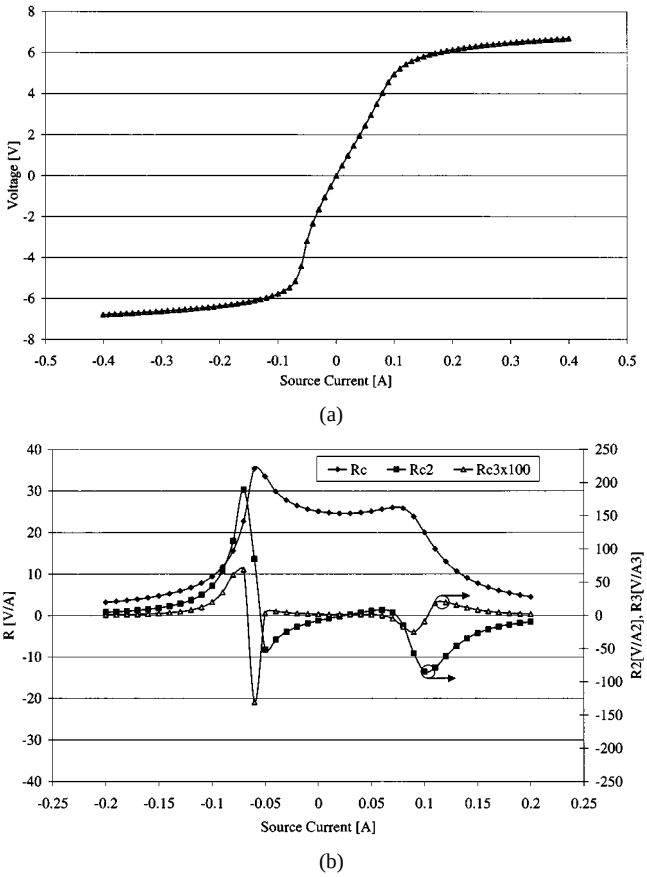

Fig. 2. (a) Illustrative characteristic function of the nonlinearity used in the circuit under study. (b) Taylor series expansion coefficients versus bias points.

purely resistive for the fundamental signals (ω_1 or ω_2) and the third harmonics ($3\omega_1$ or $3\omega_2$) as follows:

$$\begin{aligned} Z_{\mathrm{LOAD}}(\omega_2 - \omega_1) &= 2.5 + j49.9\ \Omega \\ Z_{\mathrm{LOAD}}(\omega_1) &= Z_{\mathrm{LOAD}}(\omega_2) = 50\ \Omega \\ Z_{\mathrm{LOAD}}(2\omega_1) &= Z_{\mathrm{LOAD}}(2\omega_2) = 2.5 + j49.9\ \Omega \\ Z_{\mathrm{LOAD}}(3\omega_1) &= Z_{\mathrm{LOAD}}(3\omega_2) = 50\ \Omega. \end{aligned}$$

Harmonic-balance simulated results reported in Fig. 3(a) and (b) refer to the first quiescent point: the small-signal IMD sweet spot where $R_{c3} \approx 0$ [$I_s = 60$ mA in Fig. 2(b)]. As can be observed from Fig. 3(a), the IMD presents an asymmetry in the small-signal regime, which vanishes when the operation becomes saturated. The reason for that is clear from Fig. 3(b), where the real $V_R(2\omega_2 - \omega_1)$, $V_R(2\omega_1 - \omega_2)$ and imaginary $V_I(2\omega_2 - \omega_1)$, $V_I(2\omega_1 - \omega_2)$ (normalized to $V_R(2\omega_2 - \omega_1)$ and $V_R(2\omega_1 - \omega_2)$, respectively) parts of IMD are shown. There we can see that the progressive increase of the IMD real part (equal for upper and lower IMD and sensed when LS IMD becomes important), rapidly masks the differences of the IMD imaginary parts, thus obviating any IMD asymmetry at large-signal levels.

The device was then biased at $I_S = 20$ mA, a quiescent point for which $R_{c3} > 0$, and thus, a large-signal IMD sweet spot is visible [see Fig. 4(a)] at a drive level of approximately 20 dBm. In this case, IMD asymmetry is only noticeable at the IMD minimum. This is a consequence of the fact that only there the IMD components' real parts are null and, thus, cannot mask

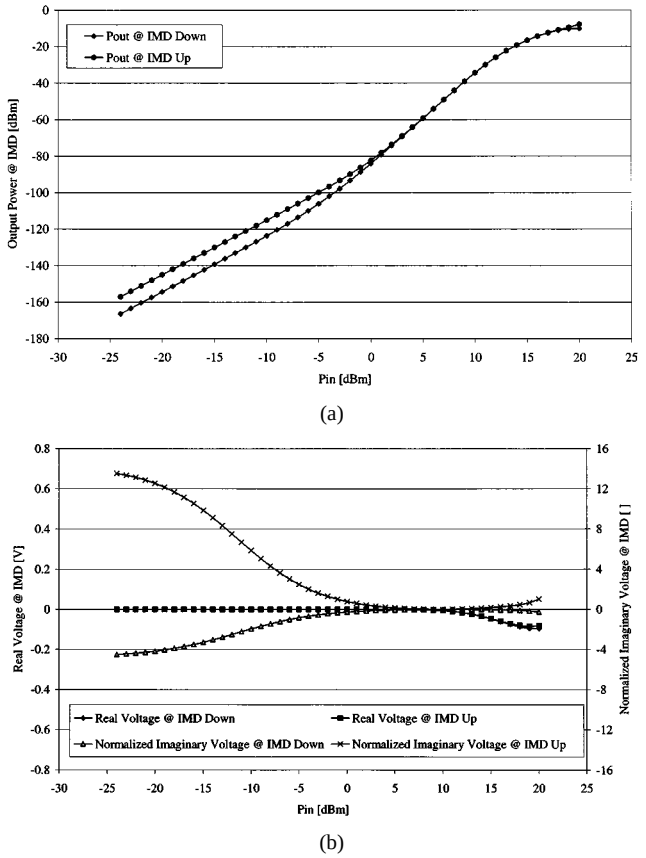

Fig. 3. (a) $P\text{in}$–$p\text{out}$ curves. (b) Corresponding real and imaginary parts of the voltage at upper and lower IMD at $I_S = 60$ mA.

the imaginary parts' differences. Fig. 4(b) validates this thought by showing the imaginary and real parts of the IMD as a function of the drive level. At the lower excitation end, the nonnull R_{c3} dominates IMD and passes its role to the also real LS IMD component when the device enters saturation.

To prove that the values of the lower and upper IMD imaginary parts determine the direction of the IMD asymmetry, we changed the baseband load from $Z_L(\omega_2 - \omega_1) = 2.5 + j49.9\,\Omega$ to $Z_L(\omega_2 - \omega_1) = 2.5 - j49.9\,\Omega$ and kept all the other terminating impedances. The results shown in Fig. 4(c) and (d) really indicate a reversing situation when compared to the previous one.

Finally, the device was biased in a point where $R_{c3} < 0$ and, thus, no large or small-signal IMD sweet spot is possible. As shown in Fig. 5(a), no asymmetry is observed in the whole Pin sweep range. According to what was already pointed out in the theoretical study (Fig. 5(b) shows that when IMD real parts dominate distortion power), IMD asymmetries are indeed impossible.

Due to the inherent differences between a multitone signal and two-tone signal and of the practical usefulness of the former, Section III will be devoted to extend these idealized conclusions to real multitone communications signals.

III. Multitone-Signal Analysis

When a nonlinear circuit is excited by a multitone signal, its in-band IMD output is no longer a single tone at $2\omega_2 - \omega_1$ or $2\omega_1 - \omega_2$, but a full band corresponding to a certain number of possible beat frequencies between the tones considered in-band

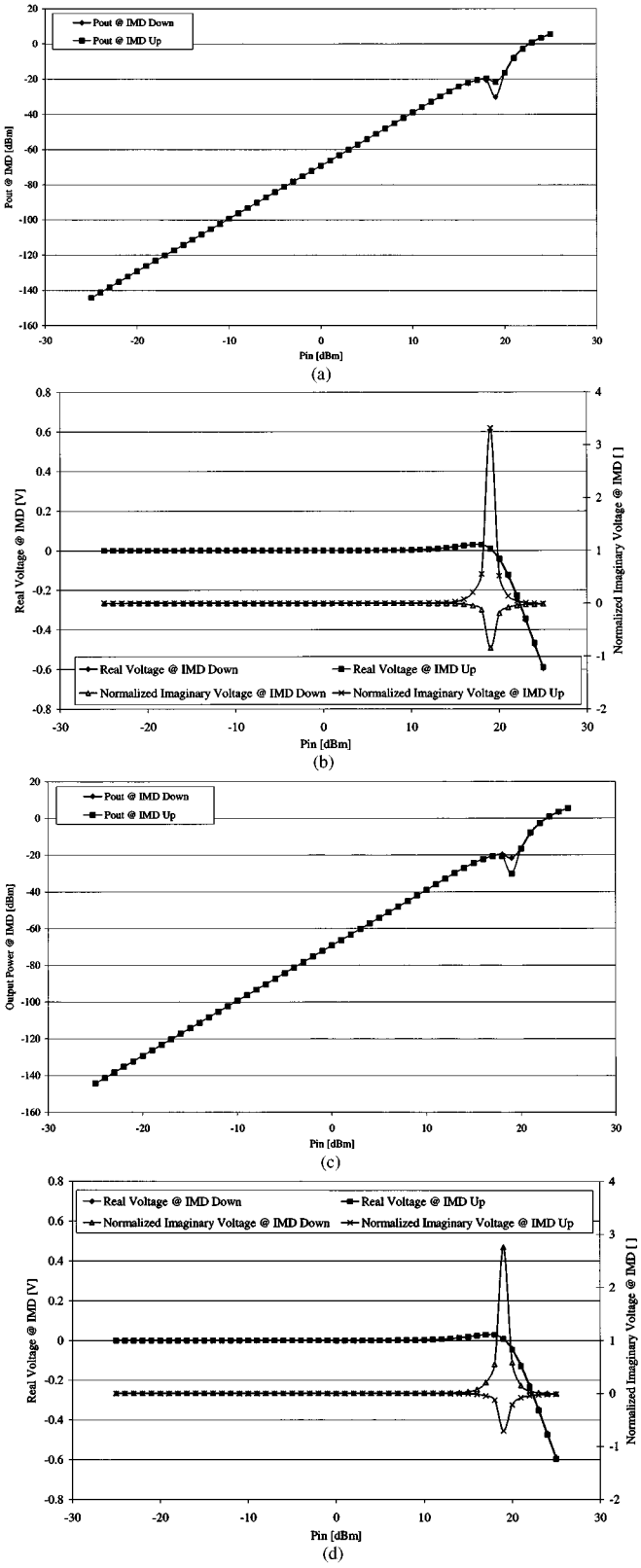

Fig. 4. $P\text{in}$–$p\text{out}$ curves and corresponding real and imaginary parts of the voltage at upper and lower IMD at $Is = 20$ mA for: (a), (b) $Z_{\text{LOAD}}(\omega_2 - \omega_1) = 2.5 + j49.9\ \Omega$ and (c), (d) $Z_{\text{LOAD}}(\omega_2 - \omega_1) = 2.5 - j49.9\ \Omega$.

[11]. For example, if an n tone signal is considered, then a generated number of $n - 1$ tones will appear in both the lower and upper adjacent bands.

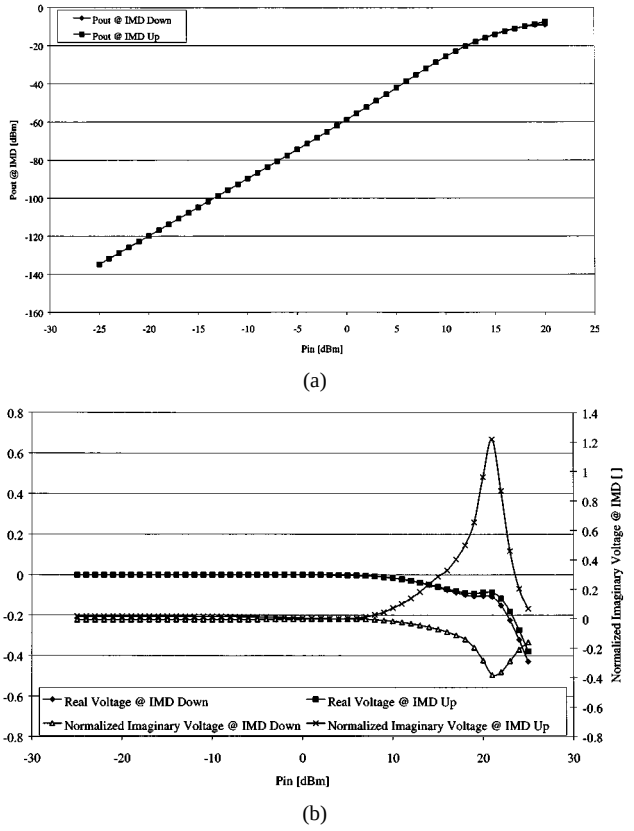

Fig. 5. (a) $P\mathrm{in}$–$p\mathrm{out}$ curves. (b) Corresponding real and imaginary parts of the voltage at upper and lower IMD $I_S = 70$ mA.

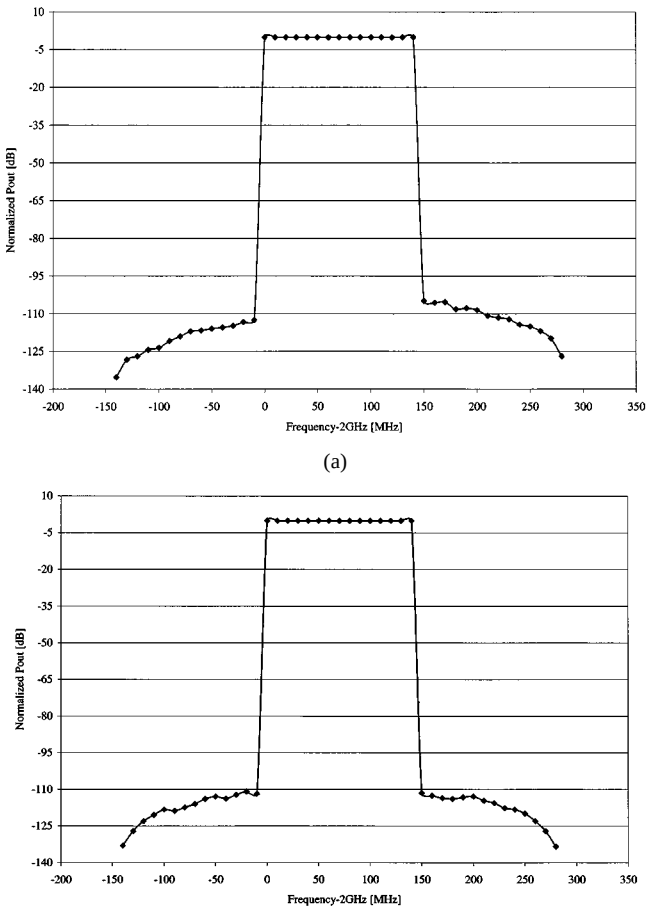

Fig. 6. Multitone output power, normalized to input power: (a) for reactive $\mathrm{ACPRu} - \mathrm{ACPRd} = 8$ dB and (b) nonreactive $\mathrm{ACPRu} - \mathrm{ACPRd} = 0$ dB baseband impedance.

In a multitone signal, the power at these adjacent bands give rise to a new nonlinear distortion figure-of-merit ACPR. ACPR relates the integrated power in the adjacent bandwidth to the transmitted signal power [12].

Two types of multitone signals can be considered. Those with equally spaced tones and some form of phase correlation between them and another one without any phase correlation. The ones with phase correlation will generate third-order nonlinear distortion that will add in voltage and not in power, while, in the other type, the generated distortion can only add in power [11]. In the Appendix, it is proven that ACPR asymmetries can be attributed to the phase correlation between tones and not to any nonlinear property of the circuit in a phase correlated multitone signal. Thus, in the following, only the phase uncorrelated signal case will be addressed.

In the general case, of a very large number of tones, this spectrum tends to narrow-band white noise. From simple calculations, as in the ones of the Appendix, it can be shown that the adjacent channel spectrum decreases in amplitude as the distortion position moves to frequencies far apart from the fundamentals. Thus, the most important mixing products are generated from different mixings at the smallest baseband $\Delta\omega = \omega_2 - \omega_1$, $\Delta\omega = \omega_3 - \omega_2$, etc., which will demand a reactive baseband impedance at very low frequencies up to dc.

In order to study the distortion induced by this excitation, the same circuit of Fig. 1 was analyzed with a multitone harmonic-balance simulator [13]. The small-signal response can be immediately extrapolated from the two-tone results since the nonlinear behavior can still be represented by a Volterra series [14].

For this analysis, the impedance at the second harmonic were considered reactive. Otherwise, no asymmetry would be visible. In Fig. 6, the circuit was biased at an IMD sweet spot, in Fig. 6(a) a reactive baseband was considered, while in Fig. 6(b) a nonreactive baseband was used. An ACPR asymmetry of nearly 8 dB can be depicted from Fig. 6(a).

To close this section, let us summarize the two main conclusions drawn.

- If there is some phase correlation between each tone in a multitone signal, the asymmetries can be attributed to the relation between each tone.
- In a multitone phase uncorrelated signal, the baseband matching circuit is responsible for the ACPR asymmetry, although now the baseband load spans from dc to the signal bandwidth.

IV. IMD Asymmetry in a Real Microwave Amplifier

To extrapolate the above conclusions to real microwave circuits and, thus, to validate them experimentally, a MESFET microwave PA and a BJT amplifier were tested for their two-tone IMD and ACPR behavior. The reason for using these two technologies refers to their distinct nonlinear distortion mechanisms [15]–[18]. In an FET, the major nonlinearity is the drain–source current, which is dependent on its gate–source and drain–source

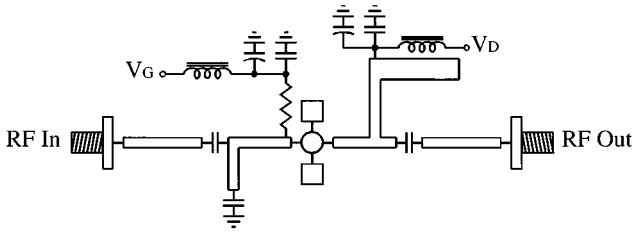

Fig. 7. Schematic diagram of the tested microwave FET PA.

voltage, whereas in bipolars, it is their emitter current, almost exclusively dependent on the base–emitter voltage, which determines IMD. Thus, while the output matching network is fundamental for the FET, in the BJT, this role is exchanged with the input termination. These different effects can be observed from the Volterra series expansion of the PA based on a MESFET (7)–(10) and Si BJT (11)–(15) active device.

A. MESFET Amplifier Analysis

Fig. 7 presents the implemented MESFET PA.

Following previous studies [15], [16], it is known that the FET's channel current nonlinearity $I_{\rm ds}(V_{\rm gs}, V_{\rm ds})$ is the most important source of nonlinear distortion, when compared to the other device's nonlinearities like gate–source and gate–drain capacitance $C_{\rm gs}(V_{\rm gs}, V_{\rm ds})$ and $C_{\rm gd}(V_{\rm gs}, V_{\rm ds})$. Other evidences gathered from these antecedent works are that $C_{\rm gs}(V_{\rm gs}, V_{\rm ds})$ varies synchronously with $I_{\rm ds}(V_{\rm gs}, V_{\rm ds})$ (and, thus, a sweet-spot condition for $I_{\rm ds}(V_{\rm gs}, V_{\rm ds}) - G_{m3} = 0$—coincides with another one for $C_{\rm gs}(V_{\rm gs}, V_{\rm ds}) - C_{g3} = 0$) and that $C_{\rm gd}(V_{\rm gs}, V_{\rm ds})$ is usually negligible when compared to the other two sources of distortion. Finally, despite the admittance values imposed by $C_{\rm gs}(V_{\rm gs}, V_{\rm ds})$ and $C_{\rm gd}(V_{\rm gs}, V_{\rm ds})$ might be important for the range of frequencies at which the amplifier will work, i.e., ω_1 or ω_2, they become completely negligible for the difference frequency. Thus, it is plausible that the nonlinear distortion created by the PA is mainly attributed to the FET's resistive nonlinearity $I_{\rm ds}(V_{\rm gs}, V_{\rm ds})$.

In this case, $H_1(\omega_1)$, $H_2(-\omega_1, \omega_2)$, and $H_3(-\omega_1, \omega_2, \omega_3)$ for the PA are equal to [8]

$$H_1(\omega) = \frac{-G_m}{1 + G_{\rm ds} Z_L(\omega)} \tag{7}$$

$$\begin{aligned} H_2(-\omega_1, \omega_2) &= \frac{-1}{2 + 2G_{\rm ds} Z_L(-\omega_1 + \omega_2)} \\ &\cdot \Big[2G_{m2} + G_{md} Z(-\omega_1) H_1(-\omega_1) \\ &\quad + G_{md} Z(\omega_2) H_1(\omega_2) \\ &\quad + 2G_{d2} H_1(-\omega_1) Z(-\omega_1) H_1(\omega_2) Z(\omega_2) \Big] \end{aligned} \tag{8}$$

$$\begin{aligned} H_3(\omega_2, \omega_2, -\omega_1) &= \frac{-1}{6 + 6G_{\rm ds} Z_L(2\omega_2 - \omega_1)} \\ &\cdot \big(6G_{m3} + 8G_{d2} Z_L(\omega_2) H_1(\omega_2) Z_L(\omega_2 - \omega_1) \\ &\quad \cdot H_2(\omega_2, -\omega_1) + 4G_{d2} Z_L(-\omega_1) H_1(-\omega_1) Z_L(2\omega_2) \\ &\quad \cdot H_2(\omega_2, \omega_2) + 6G_{d3} Z_L(\omega_2) H_1(\omega_2) Z_L(\omega_2) \\ &\quad \cdot H_1(\omega_2) Z_L(-\omega_1) H_1(-\omega_1) + 4G_{md} Z_L(\omega_2 - \omega_1) \\ &\quad \cdot H_2(\omega_2, -\omega 1) + 2G_{md} Z_L(2\omega_2) H_2(\omega_2, \omega_2) \\ &\quad + 2G_{m2d} Z_L(-\omega_1) H_1(-\omega_1) + 4G_{m2d} Z_L(\omega_2) \\ &\quad \cdot H_1(\omega_2) + 2G_{md2} Z_L(-\omega_1) H_1(-\omega_1) Z_L(\omega_2) \\ &\quad \cdot H_1(\omega_2) + 4G_{md2} Z_L(\omega_2) H_1(\omega_2) Z_L(\omega_2) H_1(\omega_2) \big) \end{aligned} \tag{9}$$

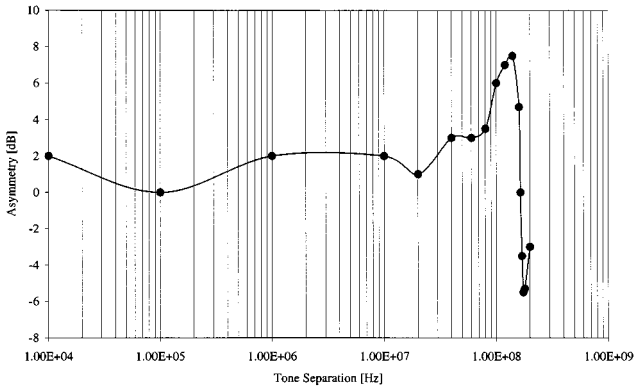

(a)

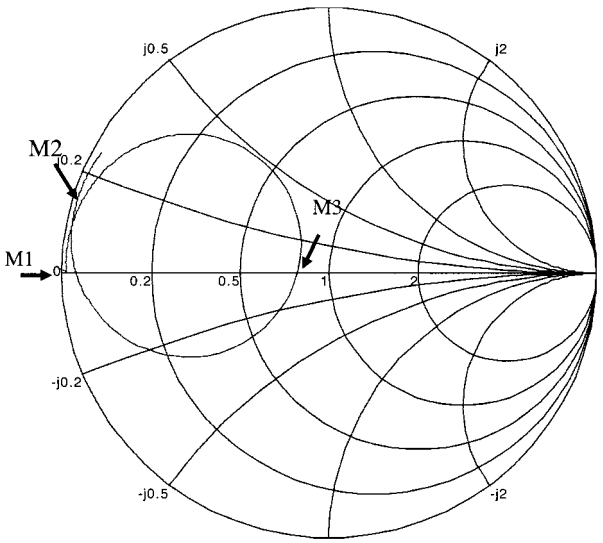

(b)

Fig. 8. (a) Experimental results of IMD asymmetry versus tone separation. (b) Experimental baseband load.

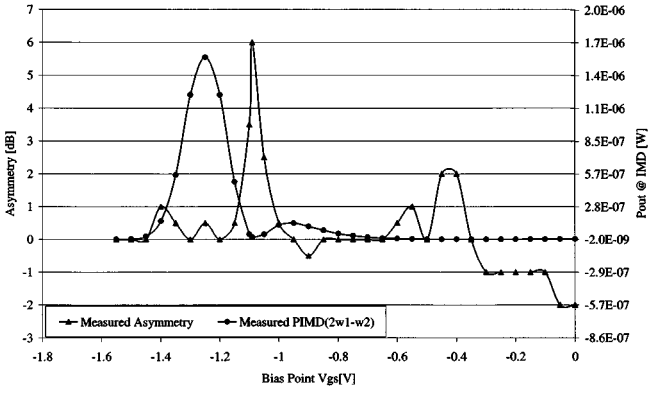

Fig. 9. Experimental results of absolute IMD power and asymmetry versus FET PA active device bias.

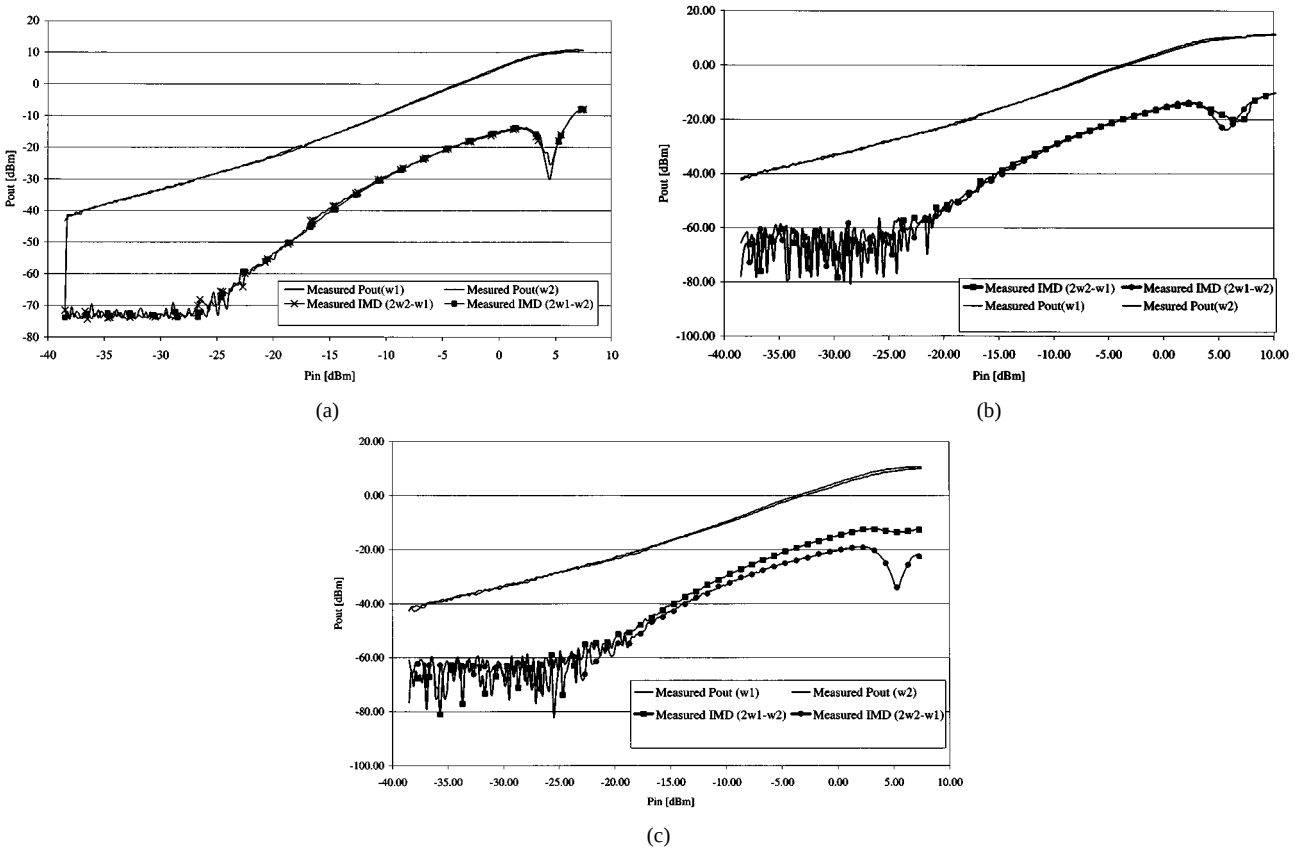

Fig. 10. Measured upper and lower fundamental and IMD power for different tone separations at a constant bias of $V_{\rm gs} = -1.2$ V. (a) 10 kHz. (b) 100 MHz. (c) 180 MHz.

The differences between $H_3(-\omega_1, \omega_2, \omega_2)$ and $H_3(-\omega_2, \omega_1, \omega_1)$ are

$$\begin{aligned} &H_3(\omega_2, \omega_2, -\omega_1) \\ &\quad = \text{Common part} - \frac{1}{6 + 6G_{\rm ds}Z_L(2\omega_2 - \omega_1)} \\ &\qquad \cdot \big(8G_{d2}Z_L(\omega_2)H_1(\omega_2)Z_L(\omega_2 - \omega_1)H_2(\omega_2, -\omega_1) \\ &\qquad + 4G_{md}Z_L(\omega_2 - \omega_1)H_2(\omega_2, -\omega_1)\big). \end{aligned} \tag{10}$$

where G_{m2}, G_{md}, G_{m2d}, G_{md2}, G_{d2}, $G_{\rm ds}$ are the Taylor coefficients of the nonlinear bi-dimensional expansion of $I_{\rm ds}(V_{\rm gs}, V_{\rm ds})$ [8] and $Z_L(-\omega_1 + \omega_2)$ is the output baseband load impedance.

As is clear from (10), the general conclusions obtained in Section II for small-signal IMD asymmetry with the ideal circuit are perfectly verified in this PA. In fact, the baseband component $H_2(-\omega_1, \omega_2)$ is still the main responsible for IMD asymmetry.

For testing this PA, the transistor was biased near its small-signal IMD sweet spot $G_3 = 0$, the load impedance was taken from the actual PA output matching network of Fig. 7, and the two-tone separation $\Delta\omega = \omega_2 - \omega_1$ was varied (Fig. 8).

Fig. 8(a) presents measured PA IMD asymmetry versus tone separation, while Fig. 8(b) shows baseband and second harmonic load impedance behavior along the $\Delta\omega$ sweep. When the baseband impedance is near a short circuit, i.e., $M1$, there is imperceptible asymmetry. When $\Delta\omega$ sees an impedance bigger than the one identified by $M2$ (30 MHz), the asymmetry worsens. After that, the baseband load reaches its maximum resistive value, i.e., $M3$ (165 MHz), and a minimum in the asymmetry appears again, reversing when the baseband imaginary part impedance changes sign. The second harmonic load, in turn, presents an imaginary part in the whole tone separation range, which enables IMD asymmetry, as above explained.

Next, $I_{\rm ds}(V_{\rm gs}, V_{\rm ds})$ coefficient's values of G_{mx} and G_{dx} were varied by changing the PA FET's bias point, while the tone separation was kept at a constant value of 100 MHz. Fig. 9 reports the measurement data obtained with this test.

As previously predicted from the general simple circuit analysis, measured results of Fig. 9 show that the worst situation of IMD asymmetry is verified when $G_3 = 0$, proving the phenomenon is not masked by the third-degree direct distortion sources.

A multitone signal was also used on this PA, but due to the mild impact of the second-order term compared with the third-order one, as already observed in the two-tone case, extremely low asymmetry was visible in the variation of bias points. Furthermore, recalling the ideal case previously presented, it was concluded that, in a multitone signal, the baseband matching networks should be reactive from dc until the bandwidth of the signal, while in the two-tone case, it can be reactive at only the difference frequency. From Fig. 8, it is possible to see that the baseband network can be considered reactive for $\Delta\omega > 30$ MHz, which will minimize the sought multitone asymmetry.

The second test was developed by sweeping the input power from its small signal to saturation behavior. The PA was biased at two different points. The first one, at $V_{\rm gs} = -1.2$ V (Fig. 10), will generate a large-signal IMD sweet spot [9], while for the

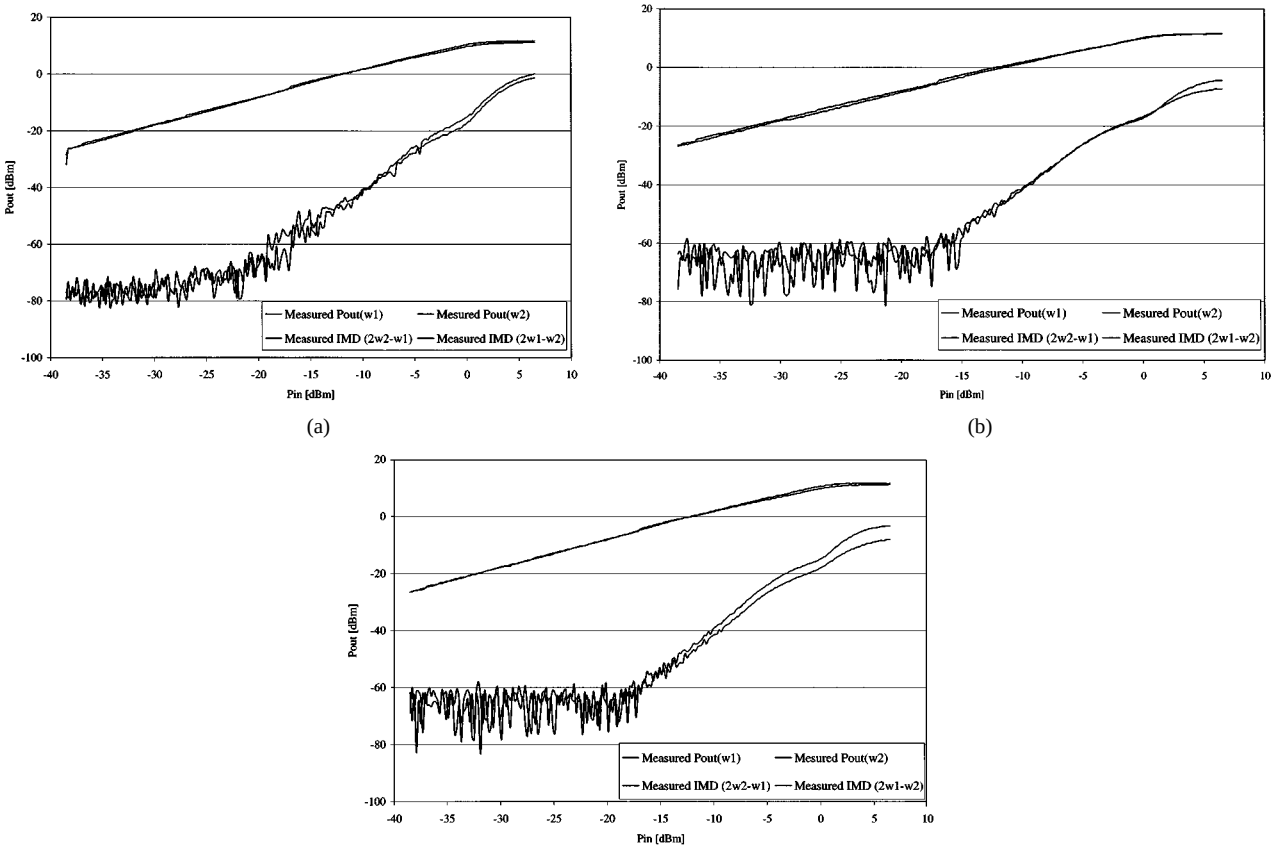

Fig. 11. Measured upper and lower fundamental and IMD power for different tone separations at a constant bias of $V_{\rm gs} = -0.68$ V. (a) -10 kHz. (b) -100 MHz. (c) -180 MHz.

other, at $V_{\rm gs} = -0.68$ V (Fig. 11), IMD power will monotonically increase with drive level.

Two-tone frequency separations tested were selected as $\Delta\omega_1 = 10$ kHz, $\Delta\omega_2 = 100$ MHz. and $\Delta\omega_3 = 180$ MHz. $\Delta\omega_1(\Delta\omega_1 < 30$ MHz) corresponds to $Z_L(\Delta\omega_1)$ near a short circuit [see Fig. 8(b)], thus obviating any IMD asymmetry. $\Delta\omega_2(30\,\text{MHz} < \Delta\omega_2 < 165\,\text{MHz})$ corresponds to a significantly inductive $Z_L(\Delta\omega_2)$ enabling a clear IMD asymmetry. Finally, $\Delta\omega_3(\Delta\omega_3 > 165\,\text{MHz})$ is such that $Z_L(\Delta\omega_3)$ is already capacitive, which leads to a reversal on the observed IMD asymmetry.

As expected, no IMD asymmetry is visible for $\Delta\omega_1 = 10$ kHz [see Fig. 10(a)].

For $\Delta\omega_2 = 100$ MHz [see Fig. 10(b)], distortion asymmetry only appears at the large-signal IMD sweet spot, which is consistent with the developed theory.

Finally, when the tone separation is $\Delta\omega_3 = 180$ MHz [see Fig. 10(c)], the IMD asymmetry presents a small constant value in almost all the swept values, except at the large-signal IMD sweet spot where it suffers a distinct increase. Despite the apparent similarity of the results obtained for $\Delta\omega_2$ and $\Delta\omega_3$, a closer observation of Fig. 10(b) and (c) indicates that, as predicted, the IMD asymmetry is really reversed. The residual asymmetry observed out of the sweet spot can be attributed to the linear characteristics of the PA. For such a large tone separation, the upper and lower fundamental powers are no longer equal at the drain because of the amplitude variation of the amplifier's linear transfer function.

According to what was done to the $V_{\rm gs} = -1.2$ V bias, Fig. 11 presents measured results for the upper and lower IMD versus input power, when the PA cannot present any large-signal IMD sweet spot ($V_{\rm gs} = -0.68$ V) and for the same three different tone separations [see Fig. 11(a)–(c)].

As theoretically predicted, Fig. 11 shows no IMD asymmetry for all tone separations tested. The constant asymmetry seen for $\Delta\omega_3 = 180$ MHz is again caused by the PA linear frequency characteristics.

B. Bipolar Amplifier Analysis

Fig. 12 presents the implemented BJT amplifier, with its equivalent BJT model description.

According to previously published studies [17], [18], it is known that the bipolar emitter current nonlinearity

$$\begin{aligned} i_E(v_{BE}) =& I_{ES}\left(e^{v_{BE}/(\eta V_T)} - 1\right) \\ \approx& I_{E0} + G_e v_{be} + G_{e2} v_{be}^2 + G_{e3} v_{be}^3 \end{aligned} \tag{11}$$

is the most important source of nonlinear distortion when compared to the other device's nonlinearities, like nonlinear emitter junction charges $C_e(V_{\rm gs}, V_{\rm ds})$. This is especially true at frequencies much lower than the BJT transition frequency, where the device was used in our experiments.

Considering only that nonlinear contribution and the simplified amplifier equivalent circuit of Fig. 12, the Volterra series nonlinear operators were derived. The output variable is V_o, while the input is V_S.

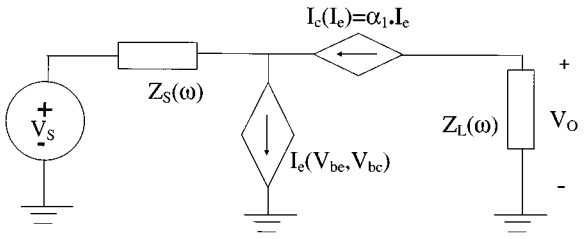

Fig. 12. Simplified bipolar amplifier equivalent circuit.

In this case, $H_1(\omega_1)$, $H_2(-\omega_1,\omega_2)$, and $H_3(-\omega_1,\omega_2,\omega_2)$ for the bipolar PA are equal to (12)–(14), shown at the bottom of this page. Similarly to the conclusions drawn for the FET amplifier, the difference between $H_3(\omega_2,\omega_2,-\omega_1)$ and $H_3(\omega_1,\omega_1,-\omega_2)$ is due to the baseband termination (15) [3]

$$H_3(\omega_2,\omega_2,-\omega_1) = \text{Commom part} - \frac{Z_L(2\omega_2-\omega_1)\alpha_1}{1+G_eZ_S(2\omega_2-\omega_1)(1-\alpha_1)}\frac{2G_{e2}}{3} \cdot\left[\frac{2Z_S(\omega_2-\omega_1)(1-\alpha_1)H_2(\omega_2,-\omega_1)}{\alpha_1 Z_L(\omega_2-\omega_1)} + \frac{2Z_S(\omega_2-\omega_1)Z_S(\omega_1)(1-\alpha_1)^2H_2(\omega_2,-\omega_1)H_1(\omega_2)}{\alpha_1^2 Z_L(\omega_2-\omega_1)Z_L(\omega_1)}\right]. \quad (15)$$

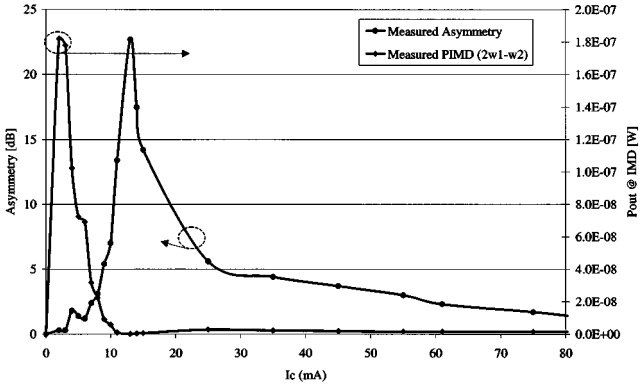

Fig. 13. Experimental results of absolute IMD power and asymmetry versus BJT PA collector current bias.

However, contrary to that device, in the BJT circuit, it is the source impedance $Z_S(\Delta\omega)$, which will determine IMD asymmetry effects. The first tests performed on the implemented BJT amplifier prototype evaluate asymmetry variation with collector current bias, as depicted in Fig. 13, under a two-tone excitation.

From Fig. 13, it is possible to see that the asymmetry is larger when the intermodulation has a minimum, which is analogous to that already visualized in the FET PA and theoretically predicted from our circuit example.

$$H_1(\omega) = -\frac{Z_L(\omega)\alpha_1 G_e}{1+G_eZ_s(\omega)(1-\alpha_1)} \quad (12)$$

$$H_2(-\omega_1,\omega_2) = -\frac{Z_L(\omega_2-\omega_1)\alpha_1 G_{e_2}}{1+G_eZ_s(\omega_2-\omega_1)(1-\alpha_1)} \cdot\left[1+\frac{Z_s(-\omega_1)(1-\alpha_1)H_1(-\omega_1)}{\alpha_1 Z_L(-\omega_1)} + \frac{Z_s(\omega_2)(1-\alpha_1)H_1(\omega_2)}{\alpha_1 Z_L(\omega_2)} + \frac{Z_s(-\omega_1)Z_s(\omega_2)(1-\alpha_1)^2H_1(-\omega_1)H_1(\omega_2)}{\alpha_1^2 Z_L(-\omega_1)Z_L(\omega_2)}\right] \quad (13)$$

$$\begin{aligned} H_3(\omega_2,\omega_2,-\omega_1) = &-\frac{Z_L(2\omega_2-\omega_1)\alpha_1}{1+G_eZ_s(2\omega_2-\omega_1)(1-\alpha_1)} \cdot\left\{\frac{2G_{e2}}{3}\left[\frac{Z_s(2\omega_2)(1-\alpha_1)H_2(\omega_2,\omega_2)}{\alpha_1 Z_L(2\omega_2)} + \frac{2Z_s(\omega_2-\omega_1)(1-\alpha_1)H_2(\omega_2,-\omega_1)}{\alpha_1 Z_L(\omega_2-\omega_1)}\right.\right. \\ &+\frac{Z_s(2\omega_2)Z_s(-\omega_1)(1-\alpha_1)^2H_2(\omega_2,\omega_2)H_1(-\omega_1)}{\alpha_1^2 Z_L(2\omega_2)Z_L(-\omega_1)} \\ &\left.+\frac{2Z_s(\omega_2-\omega_1)Z_s(\omega_1)(1-\alpha_1)^2H_2(\omega_2,-\omega_1)H_1(\omega_2)}{\alpha_1^2 Z_L(\omega_2-\omega_1)Z_L(\omega_1)}\right] \\ &+G_{e3}\left[1+\frac{2H_1(\omega_2)Z_s(\omega_2)(1-\alpha_1)}{\alpha_1 Z_L(\omega_2)} + \frac{H_1(-\omega_1)Z_s(-\omega_1)(1-\alpha_1)}{\alpha_1 Z_L(-\omega_1)}\right. \\ &+\frac{2H_1(\omega_2)H_1(-\omega_1)Z_s(-\omega_1)Z_s(\omega_2)H_1(1-\alpha_1)^2}{\alpha_1^2 Z_L(-\omega_1)Z_L(\omega_2)} \\ &+\frac{H_1(\omega_2)H_1(\omega_2)Z_s(\omega_2)Z_s(\omega_2)(1-\alpha_1)^2}{\alpha_1^2 Z_L(\omega_2)Z_L(\omega_2)} \\ &\left.\left.+\frac{H_1(\omega_2)H_1(\omega_2)H_1(-\omega_1)Z_s(\omega_2)Z_s(\omega_2)Z_s(-\omega_1)(1-\alpha_1)^3}{\alpha_1^3 Z_L(\omega_2)Z_L(\omega_2)Z_L(-\omega_1)}\right]\right\} \end{aligned} \quad (14)$$

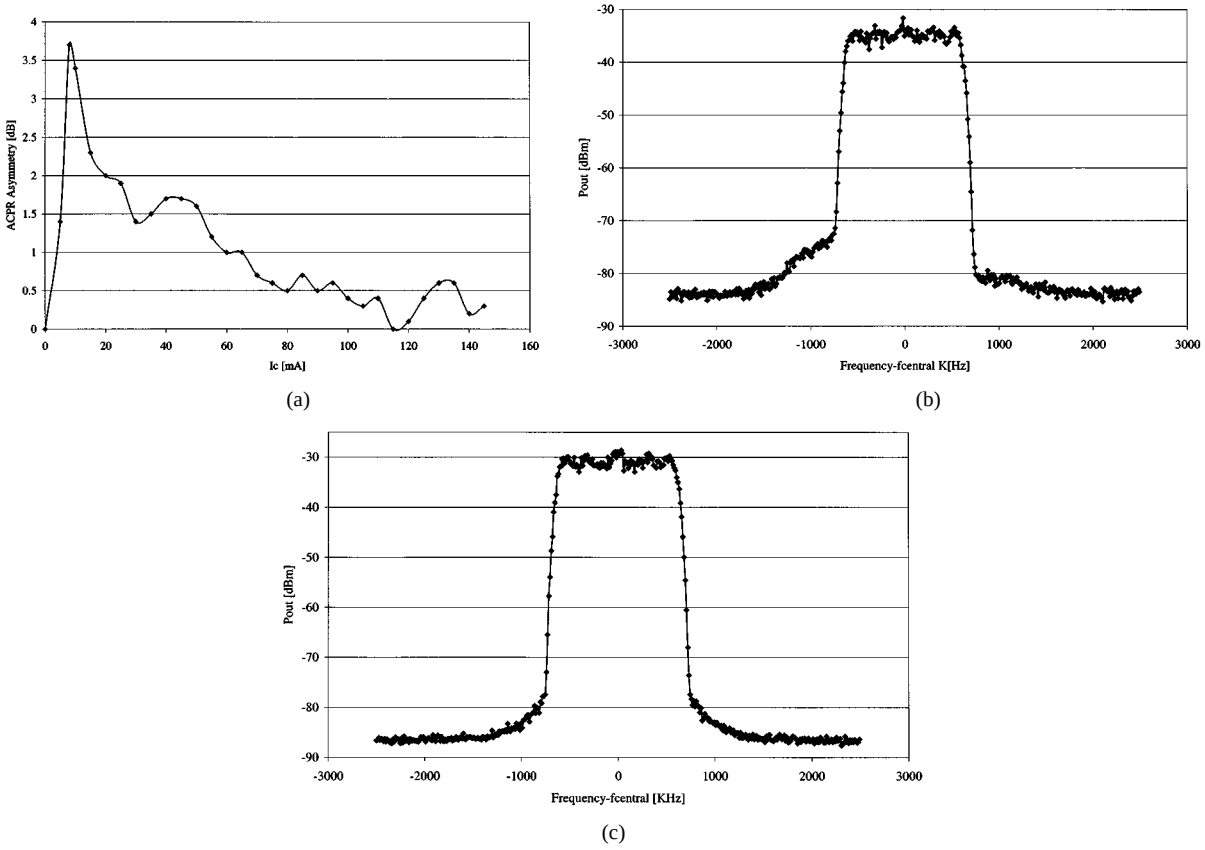

Fig. 14. Multitone asymmetry. (a) ACPR asymmetry variation with bias-point spectrum. (b) At IMD minimum. (c) At bias point greater than the IMD minimum.

The next test considers a multitone stimulus for output ACPR asymmetry measurements. Fig. 14 summarizes such results when the amplifier is operated at different bias points.

Fig. 14(a) presents the variation of ACPR asymmetry versus bias point. As expected, the overall aspect of the curve is similar to the one of Fig. 13. However, maximum ACPR asymmetry is now only 4 dB, which is clearly much smaller than the 23-dB read for the two-tone. As was already explained for the MESFET circuit, the observed lower sideband asymmetry under multitone can be attributed to the baseband matching networks that should be reactive from dc up to the signal bandwidth.

The transistor was then biased at very low IMD quiescent current equal to the minimum IMD bias point $I_c = 13$ mA in Fig. 14(b) and at a bias point much higher than that minimum $I_c = 100$ mA in Fig. 14(c). Fig. 14(b) shows a distinct difference between the upper and lower bands of the spectrum, while in Fig. 14(c), no asymmetry is visible.

The appearance of a clear ACPR asymmetry in the bipolar amplifier, contrary to what happened with the MESFET prototype, is due to the much larger second-order nonlinear effects present in a bipolar transistor. As a matter of fact, while in both devices third-order nonlinear distortion, directly originated in third-degree coefficients, come up from direct mixing of input voltages at the fundamentals, the sources of third-order distortion arising from remixing second-order distortion with the fundamentals are essentially different in those two devices.

The FETs $I_{\rm ds}(\omega_2 - \omega_1)$, $I_{\rm ds}(\omega_1 - \omega_2)$ and $I_{\rm ds}(2\omega_1)$, $I_{\rm ds}(2\omega_2)$ are created by the high G_{m2} coefficient and converted into second-order voltages at $Z_L(\omega)$. They are then remixed in the much lower cross term G_{md} with the input fundamentals or remixed in a even lower output term G_{d2} with the output fundamentals. In a bipolar amplifier, the emitter currents at the baseband and second harmonic, generated in the high G_{e2} coefficient, are instead converted into voltages at the input termination $Z_S(\omega)$ and remixed with the fundamentals again by this G_{e2} coefficient. Furthermore, since the FET is a voltage driven device, while the BJT is biased in current, the BJT source impedance at $\Delta\omega$ (near dc) will be much higher than the FET's load at this same frequency. Thus, much higher $\Delta\omega$ voltages may be expected from the BJT in comparison to the FET, even for second-order nonlinear currents of similar amplitude.

Finally, large-signal measurements were made on this amplifier, when the transistor was biased below the minimum IMD bias point and above the IMD minimum (Fig. 15).

Large-signal IMD asymmetry is visible when the transistor was biased below the minimum IMD bias point (which produces the required large-signal IMD sweet spot), while it cannot be observed for a higher bias point (for which the IMD power versus input drivel level is monotonic). The presence of large-signal IMD asymmetry only in the large-signal IMD sweet spot is in accordance with the theoretical analysis previously undertaken and the results already obtained for the FET amplifier prototype.

V. Conclusions

In this paper, a comprehensive explanation of the nonlinear phenomenon known as IMD asymmetry has been presented. First, a simple, but general, circuit was studied and used to investigate the main sources of IMD asymmetry appearing in usual

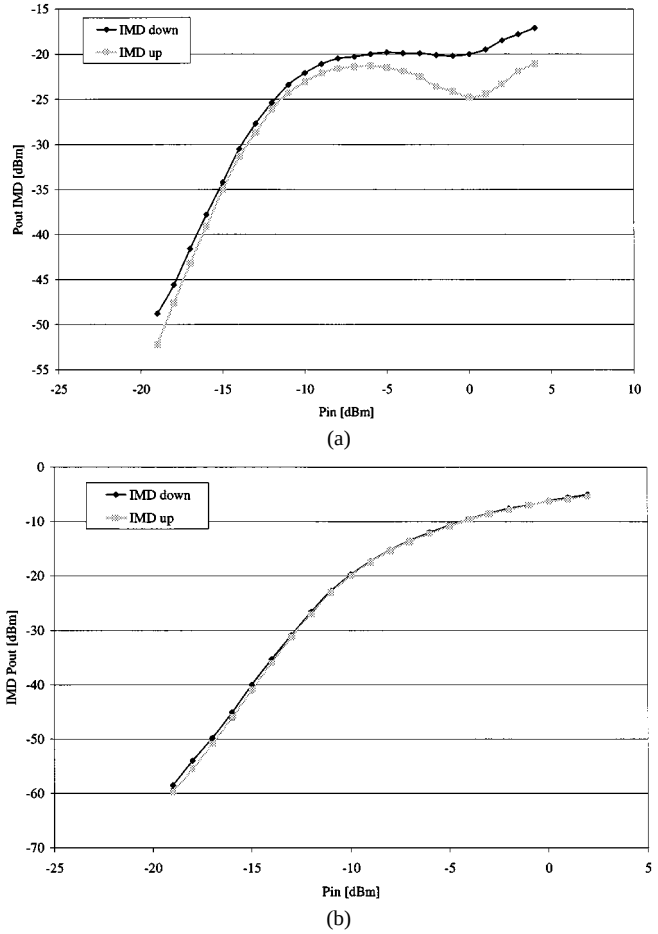

Fig. 15. Large-signal IMD asymmetry of the BJT amplifier: (a) below the IMD minimum and (b) above it.

nonlinear systems. This ideal circuit was studied for small- and large-signal operation using a combined Volterra series and describing function model. The derived necessary condition for IMD asymmetry generation was that the nonlinear device must see a significant reactive baseband load impedance, provided the real part of the IMD components do not override the imaginary parts of baseband and second harmonic contributions. These results were then extended to multitone signals, considering a phase correlated and uncorrelated multitone stimulus. The main conclusions drawn from the multitone analysis was that a certain tone phase arrangement can already create ACPR asymmetry.

These theoretical conclusions were then experimentally validated by discussing measurement data of IMD and ACPR asymmetries observed in practical microwave PAs, using two different transistor technologies, i.e., a GaAs MESFET and an Si BJT.

Finally and beyond the obvious help this may provide in modeling tasks and in characterizing IP_3, IMR, or ACPR, it is believed that this study also made viable designing PAs with a prescribed IMD asymmetry pattern. In fact, by selecting the proper baseband impedance and active device bias point, one should now be able to obviate or create IMD asymmetries; also, in this latter case, even to select the stronger distortion sideband.

APPENDIX

Here it is proven that multitone ACPR asymmetries can also be due to phase correlation present in the excitation spectrum and not to any real nonlinear property. For that, consider a simple case of a four-tone signal with phase correlation $\omega_i = \omega_o + (i-1)\Delta\omega$ and $i = 1, 2, 3, 4$ applied to a third-order nonlinearity.

TABLE I
DIFFERENT COMBINATIONS OF THIRD-ORDER MIXINGS

Lower adjacent tones			Upper adjacent tones		
ω_{l1}	ω_{l2}	ω_{l3}	ω_{u3}	ω_{u2}	ω_{u1}
$2\omega_1-\omega_4$	$\omega_1+\omega_2-\omega_4$ $2\omega_1-\omega_3$	$\omega_1+\omega_3-\omega_4$ $\omega_1+\omega_2-\omega_3$ $2\omega_1-\omega_2$ $2\omega_2-\omega_4$	$\omega_4+\omega_3-\omega_2$ $\omega_4+\omega_2-\omega_1$ $2\omega_4-\omega_3$ $2\omega_3-\omega_1$	$\omega_3+\omega_4-\omega_1$ $2\omega_4-\omega_2$	$2\omega_4-\omega_1$

The different tones are considered of equal amplitude and with different, but correlated phases $\phi_1 = 0°$, $\phi_2 = 0°$, $\phi_3 = 0°$, and $\phi_4 = 180°$. Table I describes the various third-order mixing components producing distortion in the upper and lower sidebands.

The first conclusion that can be drawn from Table I is that the first nonlinear distortion components at ω_{u3} or ω_{l3} are stronger than the other terms since they have many more mixing terms falling there. Thus, they will play a major role in determining the final ACPR values. This fact is well known in multitone distortion, as the output spectrum presents a rolloff on the spectral regrowth, which decays from the innermost to the outermost components.

As a consequence, the lower difference frequencies $\omega_2 - \omega_1$, $\omega_3 - \omega_2$, and $\omega_4 - \omega_3$ have a greater impact on this mixing terms, which requires the baseband impedance to be reactive just from very low frequencies if a measurable amount of asymmetry is sought.

The other conclusion is that, since the different distortion contributions add in voltage and not in power, a precise selection of phases can eliminate some terms, thus creating another kind of distortion asymmetry. As an illustration, if the input tones have an amplitude of A (Volt)—in the case of the phase arrangement considered above—the voltage at the most important terms equals $V\omega_{u3} = 0\,\mathrm{V}$ and $V\omega_{l3} = -6\,\mathrm{A}^3\mathrm{V}$.

ACKNOWLEDGMENT

The authors would like to acknowledge the comments and suggestions provided by J. F. Sevic, and the suggestions made by one of the reviewers about the impact of self-heating and trapping effects in asymmetries.

REFERENCES

[1] W. Bosch and G. Gatti, "Measurement and simulation of memory effects in predistortion linearizers," *IEEE Trans. Microwave Theory Tech.*, vol. 37, pp. 1885–1890, Dec. 1989.

[2] J. F. Sevic, K. L. Burguer, and M. B. Steer, "A novel envelope-termination load–pull methods for ACPR optimization of RF/microwave power amplifiers," in *IEEE MTT-S Int. Microwave Symp. Dig.*, Baltimore, MD, 1998, pp. 601–605.

[3] V. Aparin and C. Persico, "Effect of out-of-band terminations on intermodulation distortion in common-emitter circuits," in *IEEE MTT-S Int. Microwave Symp. Dig.*, Anaheim, CA, 1999, pp. 977–980.

[4] F. Sechi, "Linearized class-B transistor amplifiers," *IEEE J. Solid-State Circuits*, vol. SC-11, pp. 264–270, Apr. 1976.

[5] N. Borges de Carvalho and J. C. Pedro, "Two-tone IMD asymmetry in microwave power amplifiers," in *IEEE MTT-S Int. Microwave Symp. Dig.*, Boston, MA, 2000, pp. 445–448.

[6] P. M. McIntosh and C. M. Snowden, "The effect of a variation in tone spacing on the intermodulation performance of class A & class AB HBT power amplifiers," in *IEEE MTT-S Int. Microwave Symp. Dig.*, 1997, pp. 371–374.
[7] K. Lu, P. McIntosh, C. Snowden, and R. Pollard, "Low-frequency dispersion and its influence on the intermodulation performance of AlGaAs/GaAs HBT's," in *IEEE MTT-S Int. Microwave Symp. Dig.*, San Francisco, CA, 1996, pp. 1373–1376.
[8] J. C. Pedro, "Evaluation of MESFET nonlinear intermodulation distortion reduction by channel-doping control," *IEEE Trans. Microwave Theory Tech.*, vol. 45, pp. 1989–1997, Nov. 1997.
[9] N. Borges de Carvalho and J. C. Pedro, "Large and small signal IMD behavior of microwave power amplifiers," *IEEE Trans. Microwave Theory Tech.*, vol. 47, pp. 2364–2374, Dec. 1999.
[10] E. Ballesteros, F. Pérez, and J. Pérez, "Analysis and design of microwave linearized amplifiers using active feedback," *IEEE Trans. Microwave Theory Tech.*, vol. 36, pp. 499–504, Mar. 1988.
[11] J. C. Pedro and N. Borges de Carvalho, "On the use of multi-tone techniques for assessing RF components' intermodulation distortion," *IEEE Trans. Microwave Theory Tech.*, vol. 47, pp. 2393–2402, Dec. 1999.
[12] P. Kenington, *High-Linearity RF Amplifier Design*. Norwood, MA: Artech House, 2000.
[13] N. Borges de Carvalho and J. C. Pedro, "Multitone frequency domain simulation of nonlinear circuits in large and small signal regimes," *IEEE Trans. Microwave Theory Tech.*, vol. 46, pp. 2016–2024, Dec. 1998.
[14] S. A. Maas, "Volterra analysis of spectral regrowth," *IEEE Microwave Guided Wave Lett.*, vol. 7, pp. 192–193, July 1997.
[15] J. A. Garcia, A. Mediavilla, J. C. Pedro, N. Borges de Carvalho, A. Tazón, and J. L. Garcia, "Characterizing the gate to source nonlinear capacitor role on GaAs FET IMD performance," *IEEE Trans. Microwave Theory Tech.*, vol. 46, pp. 2344–2355, Dec. 1998.
[16] J. C. Pedro and J. Perez, "A novel nonlinear GaAs FET model for intermodulation analysis in general purpose harmonic balance simulators," in *Proc. 23rd Eur. Microwave Conf.*, Madrid, Spain, Sept. 1993, pp. 714–716.
[17] S. Narayanan and H. Poon, "An analysis of distortion in bipolar transistors using integral charge control model and Volterra series," *IEEE Trans. Circuit Theory*, vol. CT-20, pp. 341–351, July 1973.
[18] S. Maas, B. Nelson, and D. Tait, "Intermodulation in heterojunction bipolar transistors," *IEEE Trans. Microwave Theory Tech.*, vol. 40, pp. 442–448, Mar. 1992.

Nuno Borges de Carvalho (S'92–M'00) was born in Luanda, Portugal, in 1972. He received the Diploma and Doctoral degrees in electronics and telecommunications engineering from the Universidade de Aveiro, Aveiro, Portugal, in 1995 and 2000, respectively.

From 1997 to 2000, he was an Assistant Lecturer at the Universidade de Aveiro, and is currently an Auxiliary Professor and a Senior Research Scientist with the Instituto de Telecomunicações. His main research interests include computer-aided design (CAD) and measurement of nonlinear circuits and design of RF-microwave PAs.

Mr. Borges de Carvalho is a member of the Portuguese Engineering Association. He was the recipient of the 1995 Universidade de Aveiro Prize and the Portuguese Engineering Association Prize for the best 1995 student at the Universidade de Aveiro, the 1998 Student Paper Competition (third place) presented at the IEEE International Microwave Symposium, and the 2000 Institution of Electrical Engineers (IEE), U.K., Measurement Prize.

José Carlos Pedro (S'90–M'95–SM'99) was born in Espinho, Portugal, on March 7, 1962. He received the Diploma and Doctoral degrees in electronics and telecommunications engineering from the Universidade de Aveiro, Aveiro, Portugal, in 1985 and 1993, respectively.

From 1985 to 1993, he was an Assistant Lecturer with the Universidade de Aveiro, in 1993, he was a Professor, and he is currently an Associate Professor with the Universidade de Aveiro and a Senior Research Scientist at the Instituto de Telecomunicações. His main scientific interests include active device modeling and the analysis and design of various nonlinear microwave and opto-electronics circuits, particularly, the design of highly linear multicarrier PAs and mixers. He has authored or coauthored several papers in international journals and symposia.

Dr. Pedro served as a reviewer for the IEEE TRANSACTIONS ON MICROWAVE THEORY AND TECHNIQUES and the IEEE Microwave Theory and Techniques Society (IEEE MTT-S) International Microwave Symposium (IMS). He was the recipient of the 1993 Marconi Young Scientist Award and the 2000 Institution of Electrical Engineers (IEE), U.K., Measurement Prize.